RESEARCH PAPER

A hydromechanical model for unsaturated soils based on state boundary hypersurface

Dongjie Hua[1,2] · Guohua Zhang[1] · Ruyan Liu[2] · Qinghui Jiang[2] 🆔

Abstract

This paper presents an elastoplastic model to estimate the hydromechanical behavior of unsaturated soils based on state boundary hypersurface. Through mechanical hypersurface, the influence of saturation on yield stress can be expressed in a full form rather than an incremental form. Two hydraulic hypersurfaces and one mechanical hypersurface are proposed to establish the model. Two hydraulic hypersurfaces, composed of degree of saturation, void ratio and matrix suction, define the plastic hydraulic boundary. The elastic hydraulic behavior of unsaturated soils can be represented by scanning lines between these two hydraulic hypersurfaces. The mechanical hypersurface, composed of degree of saturation, void ratio and effective stress, defines the plastic mechanical boundary. The elastic mechanical behavior of unsaturated soils can be represented by scanning lines below the mechanical hypersurfaces. A large number of laboratory tests are used to validated the proposed model, showing that it can reasonably capture important features of the hydromechanical behavior of unsaturated soils.

Keywords Constitutive model · Hydromechanical · Hypersurface · Unsaturated soils

List of symbols

a	Air-entry suction for the hydraulic hypersurface
a_d	Air-entry suction for the main drying hypersurface
a_w	Air-entry suction for the main wetting hypersurface
D_{50}	Pore diameter with 50% of the total cumulative pore volume
df_{LC}	Increment of movement of LC yield surface
dV	Increment of volume of pores
$d\chi$	Increment of shifting of PSD
$f(r)$	Probability density function of pore radius
$f_i(r)$	Probability density function of pore radius after loading step i
$\tilde{f}_i(r')$	Assumed probability density function of pore radius after loading step i
$F(r)$	Distribution function of pore radius
$\tilde{F}_i(r)$	Assumed distribution function of pore radius after loading step i
f_{LC}	The location of LC yield surface.
$g(s)$	Probability density function of matric suction
$g_i(s)$	Probability density function of matric suction after loading step i
$G(s)$	Distribution function of matric suction
$G_0(s)$	Reference distribution function of matric suction
h	Parameter to indicate the amount of PSD shifting
LC	Load–collapse yield surface
NCL	Normal consolidation line
$p - u_a$	Mean net stress
p^*	Effective stress for unsaturated soils
PSD	Pore size distribution
q	Deviatoric stress
r	Radius of pore in unsaturated soils
D_{50}	Pore diameter with 50% of the total cumulative pore volume
$D_{50,0}$	Reference D_{50}
D_p	Pore diameter
e	Void ratio
e_{trial}	Trail void ratio
e_0	Reference void ratio
e_i	Void ratio after loading step i
e_p	Mechanical hypersurface

✉ Qinghui Jiang
    jqh1972@whu.edu.cn

1   Faculty of Engineering, China University of Geosciences, 430074 Wuhan, People's Republic of China

2   School of Civil Engineering, Wuhan University, 430072 Wuhan, People's Republic of China

e_m	Parameter to describe mechanical hypersurface
s	Matric suction
SWCC	Soil–water characteristic curve
t_i	Parameter to describe evolution of PSD
T	Surface tension of water
SD	Suction-decrease yield surface
SI	Suction-increase yield surface
S_r	Degree of saturation
$S_{r,d}$	Main drying hydraulic hypersurface
$S_{r,w}$	Main wetting hydraulic hypersurface
$S_{r,trial}$	Trail saturation
v	Specific volume
α	Parameter to describe mechanical hypersurface
α_i	Parameter to describe evolution of PSD
η_i	Pore radius change ratio of loading step i
κ	Parameter to describe mechanic scanning lines
κ	Parameter to describe mechanic scanning lines
κ_a	Parameter to describe mechanic scanning lines
κ_b	Parameter to describe mechanic scanning lines
κ_s	Parameter to describe hydraulic scanning lines
λ	Parameter to describe mechanical hypersurface
λ_a	Parameter to describe mechanical hypersurface
λ_b	Parameter to describe mechanical hypersurface
$\overline{\lambda}$	Slope of curve of $e - p^*$ in semi-log plot
λ_s	Parameter to describe the variation of saturation with suction
λ_e	Parameter to describe the variation of saturation with void ratio

1 Introduction

Since the early 1990s, a large number of constitutive models for unsaturated soils have been proposed [1, 2, 4, 5, 10, 13, 18, 19, 23–25, 27, 30, 34, 35, 38–41, 43, 45–48]. The influence of matric suction (s) on the stiffness and strength of unsaturated soils and the elastoplastic volume decrease upon wetting can be well reflected in the early models. However, the influence of the degree of saturation (S_r) on the yield curves of unsaturated soils is not directly considered in the early models. The variation of degree of saturation is usually incorporated in the framework of hydraulic hysteresis. Wheeler et al. [37] presented an elastoplastic constitutive model that fully couples hydraulic hysteresis with the mechanical behavior of unsaturated soils. The influence of degree of saturation on load–collapse (LC) yield surface and the influence of specific volume (v) on the suction-increase/decrease (SI/SD) yield surfaces have been included in this model.

Wheeler's model has been further developed by many researchers [12, 19, 24, 25, 28, 33, 42]. These hydromechanical models are able to capture the coupling feature of unsaturated soils. However, the coupling movement of LC yield surface is usually related to volumetric strain increment in those models. This makes it difficult to judge the mechanical state of unsaturated soils. Besides, the coupling parameters should be carefully chosen when yielding at the corner two yield surface. This two reason makes those models difficult to implement.

Hence, some researchers pay more attention on the influence of void ratio on hydraulic hysteresis. The coupling movement of soil–water characteristic curve (SWCC) with volumetric strain increment is expressed in another way. Gallipoli et al. [7] modeled the variation of degree of saturation of a deformable unsaturated soil in (S_r, s, v) space. This hydraulic model has been further developed by some researchers [9, 26, 32, 36, 44]. Especially, considering the change of pore-size distribution (PSD), this model was further developed by Hu et al. [9] to give the expression of the main wetting and main drying surfaces. Different air-entry suctions are used to define the two surfaces. The elastic hydraulic behavior can be represented by scanning lines between the main drying surface and the main wetting surface. The influence of void ratio on soil–water characteristic curve (SWCC) as well as the hydraulic hysteresis behavior can be well reflected by this model. Unfortunately, the mechanical part is absent in the model of Hu et al. [9].

The concept of "state boundary hypersurface" was used by Wheeler and Sivakumar [38]. The state boundary hypersurface is defined by a single equation relating several state variables. The state variables can be either stress variables or strain variables. The state boundary hypersurface can be used to build an elastoplastic constitutive model, with elastic behavior when the soil state lies inside the state boundary hypersurface and plastic behavior when the state boundary hypersurface is reached.

In this paper, the concept of "state boundary hypersurface" is adopted and is called "hypersurface" for short. To overcome the above limitations, the degree of saturation is taken as a state variable to rebuild a mechanical hypersurface. In this way, the influence of saturation on yield surface can be expressed in a full form rather than an incremental form. It becomes much easier to judge the mechanical state of Sect. 1, unsaturated soils. Hence, there are two kinds of hypersurfaces used in this paper, the hydraulic hypersurface and the mechanical hypersurface. In Sect. 2, considering the evolution of PSD, a general equation for hydraulic hypersurface is given. Then, two hydraulic hypersurfaces are used with a mechanical hypersurface to establish a constitutive model for unsaturated soils. The performance of the model is assessed by

comparisons with experimental data from literatures in Sect. 3. The discussion and conclusion are given in Sect. 4 and Sect. 5, respectively.

2 Framework of state boundary hypersurface

2.1 Hydraulic hypersurface

Experimental data showed that SWCC dependents on void ratio [7]. In other words, the degree of saturation varies with both matric suction and void ratio.

$$S_r = S_r(e, s) \tag{1}$$

where S_r is the degree of saturation, e is the void ratio, and s is the matric suction.

Therefore, the increment of degree of saturation can be divided into two parts

$$dS_r = \frac{\partial S_r}{\partial s}ds + \frac{\partial S_r}{\partial e}de \tag{2}$$

where $\frac{\partial S_r}{\partial s}$ and $\frac{\partial S_r}{\partial e}$ are the partial differences of degree of saturation with respect to matric suction and void ratio, respectively.

The void space of a soil may be regarded as a set of connected pores that are randomly distributed with the pore radius r. The smaller pores are potentially occupied with water, and the rest by air. Hence, the degree of saturation can be expressed by

$$S_r = F(r) = 1 - G(s) \tag{3}$$

where $F(r)$ is the distribution function of pore radius, representing the proportion of the volume of pores with radius less than r to the total pore volume. This function can be used to describe PSD. $G(s)$ is the distribution function of matric suction. The inner-connections of pores are ignored here for simplicity. This assumption is reasonable because the inner-connections of pores can be equivalent to several smaller pores, which can also be included in $F(r)$.

According to the capillary law [6] and Eq. 2, the relationship between the probability density function of pore radius and the probability density function of matric suction can be expressed by

$$rf(r) = sg(s) \tag{4}$$

where $f(r)$ is the probability density function of pore radius, and $f(r)dr$ represents the volume percentage of pores with radius from r to $r + dr$. $g(s)$ is the probability density function of matric suction. $f(r)$ and $g(s)$ are the derivatives of $F(r)$ and $G(s)$, respectively.

The evolution of PSD is important in analyzing the variation of degree of saturation [9]. The incremental form of evolution of PSD caused by deformation is analyzed below. If we assume that the size of all pores is equally reduced by consolidation. The volume percentage of pores with radius from r to $r + dr$ equals to the volume percentage of pores from radius from r' to $r' + dr'$(Fig. 1).

$$\tilde{f}_i(r')dr' = f_{i-1}(r)dr \tag{5}$$

where $\tilde{f}_i(r')$ is the probability density function of pore radius when assuming all the pores are equally reduced by consolidation.

Hence, the pore radius change ratio of loading step i is given by

$$\eta_i = \frac{r'}{r} = \left(\frac{e + de}{e}\right)^{1/3} \tag{6}$$

where r' is the assumed pore radius after loading step i.

Considering Eq. (5) and Eq. (6), the relationship between $\tilde{f}_i(r')$ and $f_{i-1}(r)$ is given by

$$\tilde{f}_i(r') = f_{i-1}(r'/\eta_i)/\eta_i \tag{7}$$

Thus, the assumed distribution function of pore radius is given by

$$\tilde{F}_i(r) = F_{i-1}(r/\eta_i) \tag{8}$$

where $\tilde{F}_i(r)$ is the distribution function of pore radius when assuming all the pores are equally reduced by consolidation.

However, the assumption that the size of all pores is equally reduced by consolidation is not consistent with experimental results. As plotted in Fig. 2, the experimental data of Tanaka et al. [31] on Osaka Clay show an additional left shifting of PSD when assuming that the size of all pores is equally reduced by consolidation. This discrepancy suggests that the pores are not only compressed, but also breakdown into small pores as pressure increases.
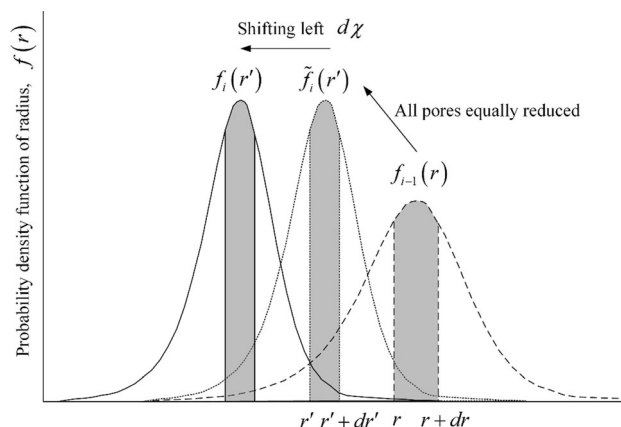

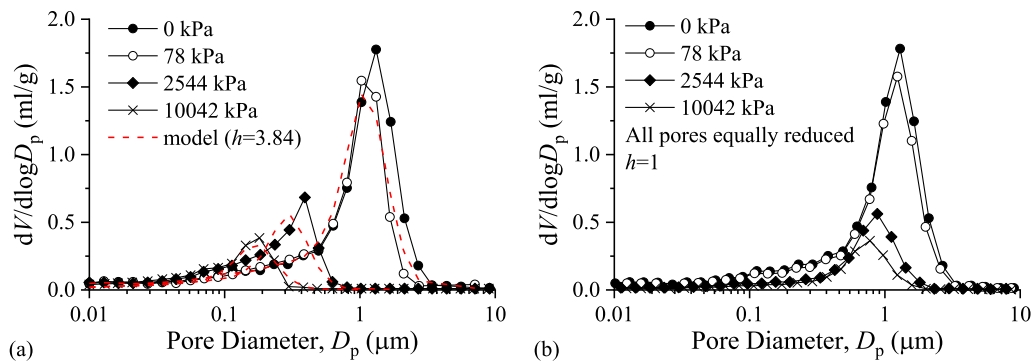Fig. 1 Evolution of probability density function of pore radius

Fig. 2 PSD for Osaka Clay under compaction. **a** experimental PSD obtained by mercury intrusion porosimetry (MIP) **b** calculated PSD under the assumption that the size of all pores is equally reduced by consolidation [31]

The stress effects on PSD and SWCC were discussed in [3, 17, 44], where the hydromechanical coupling feature of unsaturated soils can be well reflected. However, the obtained SWCC is complex when both mean net stress and matric suction are included. Hence, it is better to only included void ratio and matric suction in a hydraulic framework Eq. 1. According to the experimental results of Tanaka et al. [31] on Osaka Clay, a shifting left is added to the assumed PSD.

$$F_i(r) = F_{i-1}\left(\frac{r + d\chi}{\eta_i}\right) \tag{9}$$

where $d\chi$ indicates the amount of shifting of PSD during compression. As will be confirmed letter, $d\chi$ is given in the following form

$$d\chi = -\frac{h-1}{3e}rde \tag{10}$$

where h is a constant, $h \geq 1$. The value of h indicates the amount of PSD shifting. $h = 1$ indicates that all the pores are equally reduced and there is no additional left shifting of PSD.

According to Eq. 9 and Eq. 10, the variation of degree of saturation caused by variation of void ratio is given by

$$\frac{\partial S_r}{\partial e}de = \frac{\partial S_r}{\partial r}\frac{\partial r}{\partial e}de = -f_{i-1}(r)\frac{hr}{3e}de \tag{11}$$

where $f_{i-1}(r)$ is the probability density function of pore radius in loading step $i - 1$.

The PSD is more difficult to obtain compared with SWCC. Therefore, according to Eq. 4, Eq. 11 can be expressed by

$$\frac{\partial S_r}{\partial e}de = -sg_{i-1}(s)\frac{h}{3e}de \tag{12}$$

where $g_{i-1}(s)$ is the probability density function of matric suction in loading step $i - 1$.

Finally, the increment of degree of saturation caused by variation of matric suction and void ratio is given by

$$dS_r = \frac{\partial S_r}{\partial s}ds + \frac{\partial S_r}{\partial e}de = -g_{i-1}(s)ds - \frac{h}{3e}sg_{i-1}(s)de \tag{13}$$

Besides, according to Eq. 9 and Eq. 10, the evolution of PSD distribution function for loading step i is given by

$$F_i(r) = F_{i-1}(r\alpha_i) \tag{14}$$

where $\alpha_i = 1 - \frac{h}{3e}de$.

To give an expression of the PSD variation from a reference state, Eq. 14 can be expressed by

$$F_i(r) = F_{i-1}(r\alpha_i) = F_{i-2}(r\alpha_i\alpha_{i-1}) = \cdots \\ = F_0(r\alpha_i\alpha_{i-1}\cdots\alpha_1) \tag{15}$$

where $F_0(r)$ is the distribution function of pore radius of the reference state.

If we remark $t_i = \alpha_i\alpha_{i-1}\cdots\alpha_1$, it is easy to obtain that

$$t_i = \left(\frac{e_i}{e_0}\right)^{-h/3} \tag{16}$$

where e_i is the void ratio after loading step i and e_0 is the void ratio of the reference state.

According to Eq. 15, 16, the evolution of the distribution function of pore radius from a reference state can be given by

$$F_i(r) = F_0(rt_i) \tag{17}$$

$$f_i(r) = t_if_0(rt_i) \tag{18}$$

where $f_0(r)$ is the probability density function of pore radius of the reference state.

According to Eq. 3, the evolution of the distribution function of matric suction can be given by

$$G_i(s) = G_0(s/t_i) \tag{19}$$

$$g_i(s) = g_0(s/t_i)/t_i \tag{20}$$

where $G_0(s)$ and $g_0(s)$ are the distribution function and probability density function of matric suction of the reference state, respectively.

Considering Eq. 3 and Eq. 19, the variation of degree of saturation with matric suction and void ratio is given by

$$S_r = 1 - G_i(s) = 1 - G_0 \left[s \left(\frac{e}{e_0} \right)^{h/3} \right] \qquad (21)$$

Equation 26 gives a general expression of the variation of degree of saturation with matric suction and void ratio and $S_{r,0} = 1 - G_0(s)$ represents the SWCC curve of the reference state.

Noteworthy, the relationship of D_{50} and the void ratio can be deduced from Eq. 17.

$$0.5 = F_i(D_{50}/2) = F_0(t_i D_{50}/2) \qquad (22)$$

where D_{50} is the diameter of pore where 50% of the total cumulative porosity percentage is attained.

Hence, the relationship between D_{50} and e is given by

$$D_{50} = \left(\frac{e}{e_0} \right)^{h/3} D_{50,0} \qquad (23)$$

where $D_{50,0}$ is the value of D_{50} of the reference state.

Equation 23 indicates a linear relationship between $D_{50} - e$ in a log–log plot and the slope is $h/3$. The experimental data [31] of Osaka Clay Ma13 shows a value of $h = 1.28 \times 3 = 3.84$ Fig. 3. With the value of h, the model is capable to predict the PSD shifting of Osaka Clay Ma13 under different pressure. Noteworthy that the y axis in Fig. 2 is $dV/d \log D_p$, not the probability density function of pores $f(r)$. If we express the PSD in another way

$$\begin{cases} l(\log D_p) = dV/d \log D_p \\ L(\log D_p) = \int_{-\infty}^{\log D_p} l(\log x) d \log x \end{cases} \qquad (24)$$

where $L(\log D_p)$ represent the volume of pores with diameter smaller than D_p, dV is the increment of volume of pores. Therefore,

$$L(\log D_p) = eF(D_p/2) \qquad (25)$$
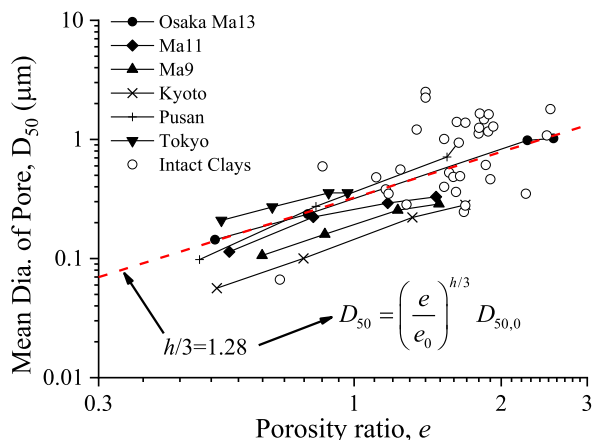
Considering Eq. 17 and Eq. 24, the evolution of PSD in terms of $l(\log D_p)$ can be represented by

$$l_i(\log D_p) = \frac{e_i}{e_0} l_0 \left(\log D_p - \frac{h}{3} \log \frac{e_i}{e_0} \right) \qquad (26)$$

where $l(\log D_p)$ is derivative of $L(\log D_p)$, $l_i(\log D_p)$ is the value of $l(\log D_p)$ in loading step i.

Take the PSD of Osaka Clay Ma13 [31] at 0 kPa as a reference state, the PSD of Osaka Clay Ma13 under 78 kPa, 2544 kPa and 10,042 kPa can be obtained by Eq. 26. As added in Fig. 2 a, the predicted PSD curves show reasonable good fit to the experimental data. Actually the assumption of all pores are equally reduced by compression is a special situation of the model with $h = 1$.

Noteworthy, the relationship of air-entry suction and void ratio can also be deduced from Eq. 21.

$$s_{ae} = \left(\frac{e}{e_0} \right)^{-h/3} s_{ae,0} \qquad (27)$$

where s_{ae} is the air-entry suction with respect to void ratio e, $s_{ae,0}$ is the value of s_{ae} in the reference state.

Equation 27 indicates a linear relationship between s_{ae} and e in log–log plot and the slope is $-h/3$. This deduction is consistent with the experimental data presented in the paper of Huang et al. [11] on touchet loam, Columbia sandy loam and unconsolidated sand Fig. 4.

Equation 23 indicates a liner relationship between $D_{50} - e$ in log–log plot Fig. 3; Eq. 26 indicates the amount of shifting of PSD in terms of $l(\log D_p)$ Fig. 2a; Eq. 27 indicates a liner relationship between $s_{ae} - e$ in log–log plot Fig. 4. These three equations are all basically derive from Eq. 10, therefore, the correctness of Eq. 10 is guaranteed.

Furthermore, if we remark $\lambda_s = -\frac{\partial S_r}{\partial \ln s}$ and $\lambda_e = -\frac{\partial S_r}{\partial \ln e}$, the degree of saturation increment is given by
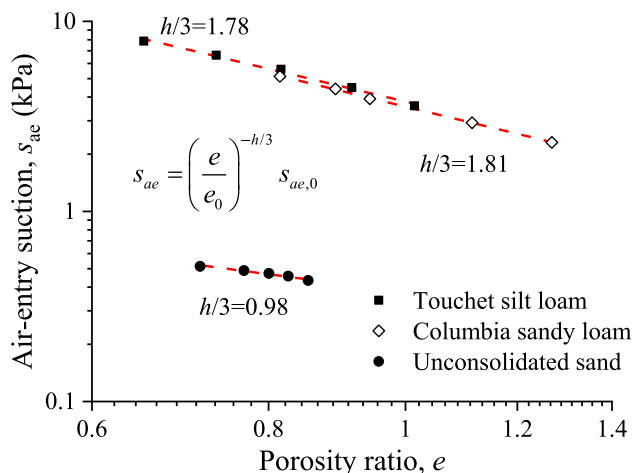

Fig. 3 Relation between D_{50} and e in log–log plot [31]

Fig. 4 Relation between s_{ae} and e in log–log plot [11]

$$dS_r = -\lambda_s d\ln s - \lambda_e d\ln e \tag{28}$$

Considering the general expression of the variation of degree of saturation with matric suction and void ratio given by Eq. 21, the following relation can be obtained

$$\lambda_e = \frac{h}{3}\lambda_s \tag{29}$$

Equation 10 and Eq. 29 show that h is an interesting parameter. In the micro scope, it indicates the amount of PSD shifting. In the macro scope, it indicates the variation of degree of saturation with void ratio. Besides, in a wide range of matric suction, experimental results show a linear relationship between $S_r - \ln s$. According to Eq. 28 and Eq. 29, there may be a linear relationship between $S_r - \ln e$. This deduction is consistent with the experimental results of Sun et al. on Pearl Clay [28], which shows a linear relationship between S_r and $\ln e$ when the soil is loaded at constant matric suction Fig. 5.

Equation 21 gives a general expression of the variation of degree of saturation with matric suction and void ratio. Any form of SWCC at a reference state can be extended to be a hypersurface in the (e, s, S_r) space to describe the variation of degree of saturation with matric suction and void ratio. This form of surface is called hydraulic hypersurface which defines the plastic hydraulic boundary of unsaturated soils. For example, if we adopt the Fredlund and Xing's [6] SWCC to describe the hydraulic hypersurface.

$$S_{r,0} = 1 - G_0(s) = \{\ln[\exp(1) + (s/a)^n]\}^{-m} \tag{30}$$

where a is the air-entry matric suction. m, n are the shape parameters of SWCC.

Extending the SWCC given by Eq. 30 to the (e, s, S_r) space by Eq. 21. The hydraulic hypersurface is given by

$$S_r = \left\{\ln\left[\exp(1) + (s/a)^n (e/e_0)^{hn/3}\right]\right\}^{-m} \tag{31}$$

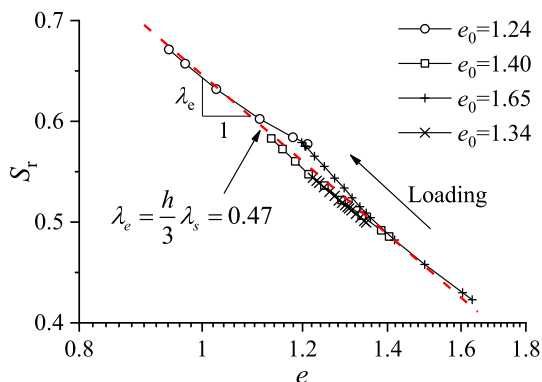Considering hydraulic hysteresis, two air-entry value are used to build the main wetting and the main drying hydraulic hypersurface.

$$S_r =$$
$$\begin{cases} \left\{\ln\left[\exp(1) + (s/a_d)^n (e/e_0)^{hn/3}\right]\right\}^{-m} & \text{main drying} \\ \left\{\ln\left[\exp(1) + (s/a_w)^n (e/e_0)^{hn/3}\right]\right\}^{-m} & \text{main weting} \end{cases}$$
$$\tag{32}$$

where a_d and a_w are the air-entry matric suction for the main drying hypersurface and the main wetting hypersurface, respectively. The shape parameters m, n are assumed to be the same for the main drying hypersurface and the main wetting hypersurface.

The hydraulic part of the constitutive model is plotted in Fig. 6. The main drying hypersurface and the main wetting hypersurface Eq. 32 define the plastic hydraulic boundary of unsaturated soils. The elastic hydraulic behavior can be expressed by scanning lines between the two hydraulic hypersurfaces. The hydraulic scanning behavior can be caused by either the variation of matric suction or by the variation of void ratio between the two hydraulic hypersurfaces. Considering Eq. 29, the hydraulic scanning line is given by

$$dS_r = -\kappa_s d\ln s - \frac{h}{3}\kappa_s d\ln e \tag{33}$$

where κ_s is the partial derivative of S_r over $\ln s$, $\frac{h}{3}\kappa_s$ is the partial derivative of S_r over $\ln e$.

The parameter κ_s is regarded as a constant in this paper, which gives a linear type of hydraulic scanning lines. Though a nonzero κ_s leads to a problem regarding the smooth transition between the unsaturated soil and saturated conditions[15], this limitation can be overcome as long as the variation of degree of saturation is strictly fixed by two smooth hydraulic hypersurfaces.
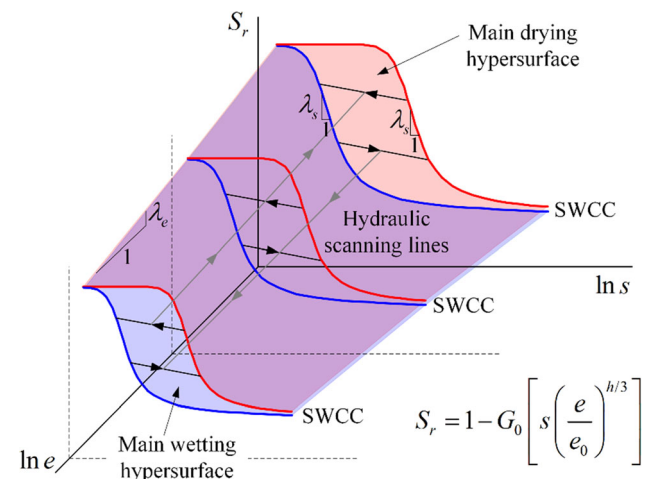

Fig. 5 Relation between S_r and e for loading at constant matric suction on Pearl Clay [28]

Fig. 6 The hydraulic part of the constitutive model in (e, s, S_r) space.

3 Mechanical hypersurface

The hydraulic part of the constitutive model is illustrated in Sect. 2.2. The variation of degree of saturation with matric suction and void ratio is governed by hydraulic hypersurfaces and hydraulic scanning lines. There should be a mechanical part to make a complete constitutive model.

The LC yield surface moves inward as degree of saturation increase and outward as degree of saturation decrease [37]. This phenomenon indicates that the normal consolidation line (NCL) moves inward as degree of saturation increases Fig. 7a. This coupling behavior has been modeled by many researchers [8, 14–16, 37]. However, most of the models related the LC yield curve movement with plastic degree of saturation increment Eq. 34. The location of LC yield surface is given in an incremental form. This makes it is difficult to judge the mechanical state of unsaturated soils. Besides, the coupling parameters should be carefully chosen when yielding at the corner of SD/SI and LC yield curve.

$$df_{LC} = df_{LC}\left(dS_r^p, \cdots\right) \qquad (34)$$

where df_{LC} is the increment of LC yield curve, dS_r^p is the increment of plastic degree of saturation.

The coupling movements of LC yield curve with degree of saturation have been considered in another way in this paper. A type mechanical hypersurface is proposed in the (S_r, p^*, e) space. Similar to the hydraulic hypersurface, it is reasonable to assume the existence of mechanical hypersurface to define the plastic mechanical boundary of unsaturated soils. In this way, the location of the LC yield surface is given in a total form.

$$f_{LC} = f_{LC}(S_r, \cdots) \qquad (35)$$

where f_{LC} is the function of LC yield curve.

The coupling parameters between LC curves and SD/SI curves are now become shape parameters of the mechanical hypersurface, where the mechanical state of the unsaturated soils can be easily obtained. In this paper, the shape of the mechanical hypersurface is given by

$$e_p = e_m + \alpha(1 - S_r) - \lambda \ln p^* \qquad (36)$$

where e_p define the mechanical boundary of unsaturated soils in (S_r, p^*, e) space., e_m is the value of e_p for a saturated soil under low confining stress ($S_r = 1, p^* = 1$), α is a shape parameter to take account the influence of degree of saturation on NCLs. λ is the slope of NCLs and is assumed to be a constant for all degree of saturations, p^* is the effective stress for unsaturated soil and is given by [37]

$$p^* = (p - u_a) + sS_r \qquad (37)$$

where $(p - u_a)$ is the mean net stress.

The mechanical elastic behavior can be expressed by scanning lines below the mechanical hypersurface. The scanning line is given by

$$de = -\frac{\kappa dp^*}{p^*} - \beta dS_r \qquad (38)$$

where κ is the partial derivative of e over $\ln p^*$; β is the partial derivative of e over S_r.

The shape of the mechanical scanning lines is plotted in Fig. 7b. The shape of the mechanical scanning lines varies with confining stress. This is because the shape parameter β varies with confining stress to give an appropriate amount of wetting collapse. A reduction in matric suction (wetting) for a given confining stress will lead to a reduction in effective stress, in the same time may also induce an irrecoverable volumetric compression (collapse). Adding parameter β in the mechanical scanning line is to consider the additional influence of saturation on void ratio, such as wetting collapse. Wetting collapse is usually accompanied with SD yielding (reached the main wetting hydraulic hypersurface), and irrecoverable increment of saturation is accompanied by an irrecoverable volumetric compression according to Eq. 38. As the confining stress is increased, the amount of collapse increases and may reach a maximum then followed by decreasing values [1]. The value of
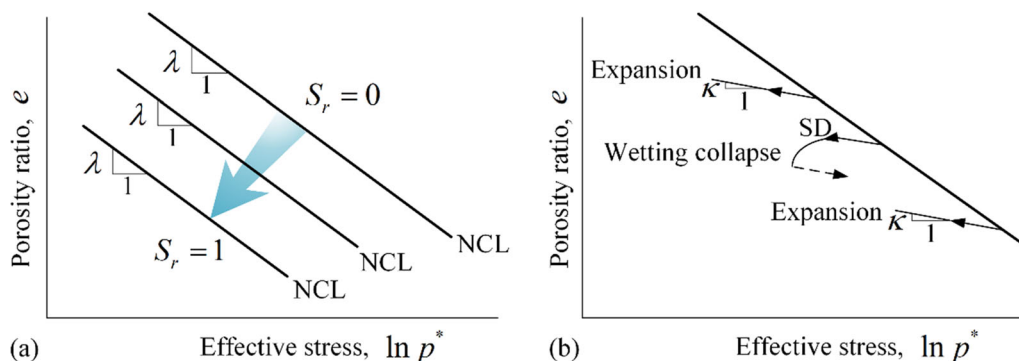

Fig. 7 Mechanical behavior of unsaturated soils. **a** Inward movement of NCLs with increase in saturation; **b** Mechanical scanning lines
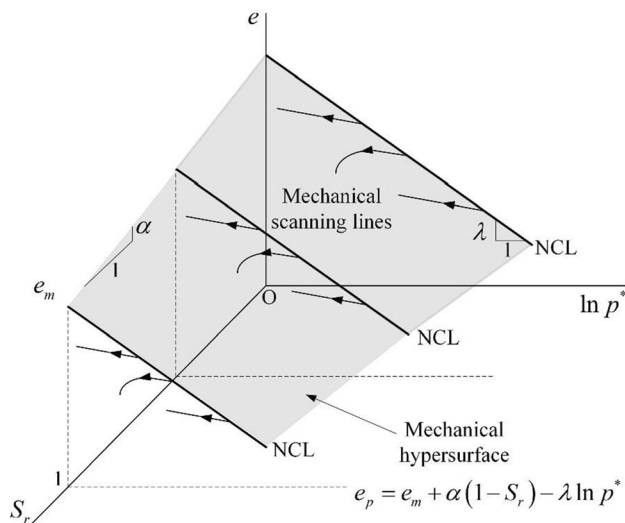
Fig. 8 The mechanical part of the constitutive model in (S_r, p^*, e) space

β may show similar tendency with confining stress $\beta = \beta(p - u_a)$. For example, a value of 0.45 is used for β when the soil is wetted at a medium stress level of 50 kPa (Test No. 12 listed in Table 5, 6). The wetting collapse behavior of bentonite–kaolin mixture is well predicted in Fig. 13g. At lower confining stress level of 10 kPa (Test No. 10, No. 11 and No.13 listed in Table 5, 6), a zero β is used to predict the elastic expansion during wetting Fig. 13a, e and i which is the same as most existing models. More experimental data are needed to calibrated the relation between the new parameter β and the confining stress.

The mechanical hypersurface and the mechanical scanning lines composite the mechanical part of the constitutive model (Fig. 8). It is more convenient to judge the mechanical state of unsaturated soils when taking degree of saturation as a state variable to build the mechanical hypersurface. The mechanical hypersurface defines the plastic mechanical boundary of unsaturated soils. The elastic mechanic behavior can be represented by mechanical scanning lines below the mechanical hypersurface.

Besides, the mechanical hypersurface given by Eq. 36 suggests that the compression curve for saturated soils obtained from wetting at different mean net stress is the same. This is consistent with the experimental results of sun et al. [29].

4 Hydromechanical modeling

The hydraulic part and the mechanical part of the constitutive model are given in Sect. 2.1 and Sect. 2.2, respectively. These two parts are used together to build a hydromechanical constitutive model for unsaturated soils. The hydraulic hypersurfaces and the mechanical hypersurface are given by Eq. 32 and Eq. 36, respectively. The hydraulic scanning line and the mechanical scanning line are given by Eq. 33 and Eq. 38, respectively. Hence, a hydromechanical model is proposed based on those hypersurfaces and scanning lines.

As listed in Table 1, the plastic behavior and elastic behavior can be represented by the hypersurfaces and scanning lines. Two hydraulic hypersurfaces define the plastic hydraulic boundary. The elastic hydraulic behavior of unsaturated soils can be represented by scanning lines between these two hydraulic hypersurfaces. The mechanical hypersurface defines the plastic mechanical boundary. The elastic mechanical behavior of unsaturated soils can be represented by scanning lines below the mechanical hypersurfaces.

The implementation of model can be started from assuming the state lies inside the scanning zone; then, the increment of effective stress, void ratio and degree of saturation can be obtained by

$$\begin{cases} dS_r = -\kappa_s d \ln s - \dfrac{h}{3}\kappa_s d \ln e \\ de = -\dfrac{\kappa dp^*}{p^*} - \beta dS_r \\ dp^* = d(p - u_a) + s dS_r + S_r ds \end{cases} \tag{39}$$

Table 1 A hydromechanical model for unsaturated soils

Hydromechanical state		Constitutive equations
Hydraulic	Hypersurfaces	$S_{r,d} = \left\{ \ln\left[\exp(1) + (s/a_d)^n (e/e_0)^{hn/3}\right] \right\}^{-m}$ (main drying)
		$S_{r,w} = \left\{ \ln\left[\exp(1) + (s/a_w)^n (e/e_0)^{hn/3}\right] \right\}^{-m}$ (main wetting)
	Scanning lines	$dS_r = -\kappa_s d \ln s - \frac{h}{3}\kappa_s d \ln e$
Mechanic	Hypersurface	$e_p = e_m + \alpha(1 - S_r) - \lambda \ln p^*$
	Scanning lines	$de = -\frac{\kappa dp^*}{p^*} - \beta dS_r$

Table 2 Model parameters for hydraulic hypersurfaces

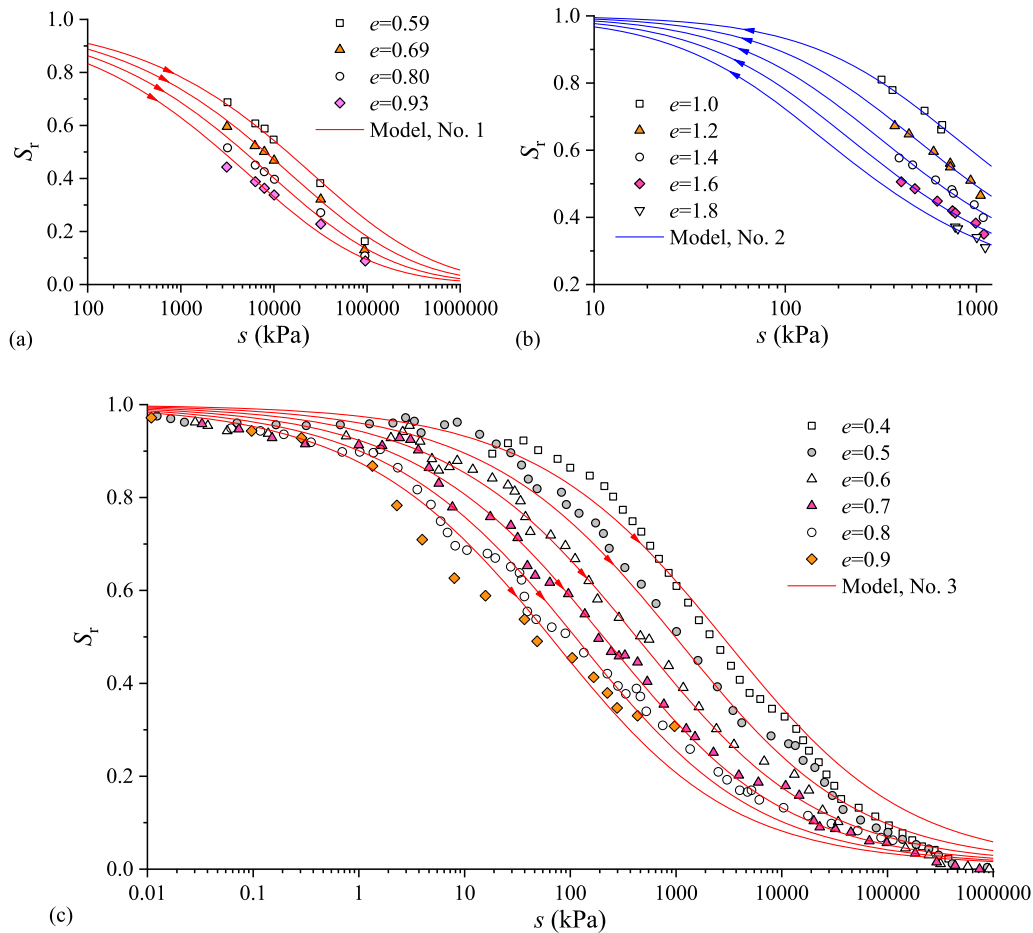| No	Soil type	Hydraulic parameters						references
		a_d(kPa)	a_w(kPa)	m	n	h	κ_s	
1	Municipal Boom clay	44,379	–	7.32	0.42	10.47	–	[20]
2	Speswhite kaolin	–	396	0.98	1.14	8.23	–	[32]
3	Clayey silty sand	55.06	–	2.85	0.45	13.91	–	[21]

Fig. 9 Measured and predicted main hydraulic drying/wetting curves for: **a** No. 1, municipal Boom clay; **b** No. 2, Speswhite kaolin; **c**No. 3 clayey silty sand

There are three unknown variables (dS_r, de, dp^*) and three independent equations in Eq. 39. By solving the linear equations given in Eq. 39, a trial degree of saturation and a trial void ratio can be written as

$$\begin{cases} S_{r,trial} = S_r + dS_r \\ e_{trial} = e + de \end{cases} \quad (40)$$

The updated soil hydraulic state $\left(e + de, s + ds, S_{r,trial}\right)$ should be located between the two hydraulic hypersurfaces.

Besides, the updated soil mechanical state $(S_r + dS_r, p^* + dp^*, e_{trial})$ should be located below the mechanical hypersurface. Therefore, the following statements are used.

If $e_{trial} > e_p$, the mechanical hypersurface instead of the mechanical scanning line is used to recalculate the increments. The increment of void ratio is given by

$$e + de = e_p(S_r + dS_r, p^* + dp^*) \quad (41)$$

Table 3 Model parameters for bentonite–kaolin under mechanical cycling [22]

No	Hydraulic parameters						Mechanical parameters				
	a_d(kPa)	a_w(kPa)	m	n	h	κ_s	e_m	α	λ	κ	β
4	–	290	0.78	0.90	25.00	0.03	2.46	0.16	0.25	0.08	–
5	–	290	0.78	0.90	25.00	0.03	2.39	0.16	0.25	0.08	–
6	–	290	0.78	0.90	25.00	0.03	2.51	0.16	0.25	0.08	–
7	–	290	0.78	0.90	25.00	0.03	2.53	0.16	0.25	0.08	–
8	–	290	0.78	0.90	25.00	0.03	2.46	0.16	0.25	0.08	–
9	–	290	0.78	0.90	25.00	0.03	2.46	0.16	0.25	0.08	–

Note: No. 4–No. 9 indicate the original test 13, test 11, test 6, test 7, test 9 and test 10 in Sharma's [22] paper

Table 4 Stress path for bentonite–kaolin under mechanical cycling [22]

No	$p - u_a$(kPa)	s(kPa)
4	10 → 100	200
5	10 → 200 → 20	100
6	10 → 94 → 10	300
7	10 → 175 → 10	300
8	10 → 100 → 10 → 250 → 100	200
9	10 → 100 → 10	200
	10	200 → 20 → 200
	10 → 200 → 20	200

Note: There are three loading stages for No. 9, two mechanical loading–unloading cycles intersected by a wetting–drying cycle

If $S_{r,trail} > S_{r,d}$, the main drying hydraulic hypersurface instead of the hydraulic scanning line is used to recalculate the increments. The increment of degree of saturation is given by

$$S_r + dS_r = S_{r,d}(e + de, s + ds) \qquad (42)$$

If $S_{r,trail} < S_{r,w}$, the main wetting hydraulic hypersurface instead of the hydraulic scanning line is used to recalculate the increments. The increment of degree of saturation is given by

$$S_r + dS_r = S_{r,w}(e + de, s + ds) \qquad (43)$$

Noteworthy that, Eq. 39 is a system of linear equations to solve the increments of effective stress, void ratio and degree of saturation. Once one or two of the hypersurfaces are reached, the increments are determined by a system of nonlinear equations, where an iterative algorithm is required.

Once the satisfied degree of saturation and void ratio at the updated state is obtained, the subsequent degree of saturation and void ratio can be easily calculated by repeating the above procedure. With mechanical hypersurface, the influence of degree of saturation on LC yield curve has been considered in a full form rather than in an incremental form. Thus, it is much easier to judge the mechanical state of unsaturated soil, and it is much easier to implement the constitutive model (only three equations are needed).

A total of eleven parameters are needed for the proposed model, including six hydraulic parameters $(a_d, a_w, m, n, h, \kappa_s)$ and five mechanical parameters $(e_m, \alpha, \lambda, \kappa, \beta)$. The parameters a_d, a_w, m, n, h can be determined by wetting–drying cycles on the main drying/wetting hypersurface. The parameter κ_s can be determined by wetting–drying tests in the hydraulic scanning zone. The parameters e_m, α, λ can be determined by loading tests on the mechanical hypersurface. The parameters κ, β can be determined by unloading test in the mechanical scanning zone. Especially, wetting collapse tests should be conducted to determine parameter β.

5 Comparison of model predictions with experimental results

In this section, several experimental results are compared with model predictions to demonstrate its usefulness. A total of 13 tests are used to validate the model. Three (No. 1 – No. 3) experiment data (municipal Boom clay [20], Speswhite kaolin [32] and clayey silty sand [21]) are used to validate the rationality of hydraulic hypersurface. The other ten experiments (No. 4 –No. 13) are used to validate the rationality of the proposed hydromechanical model. This ten tests are isotropic loading/unloading tests conducted by Sharma [22] on bentonite–kaolin.
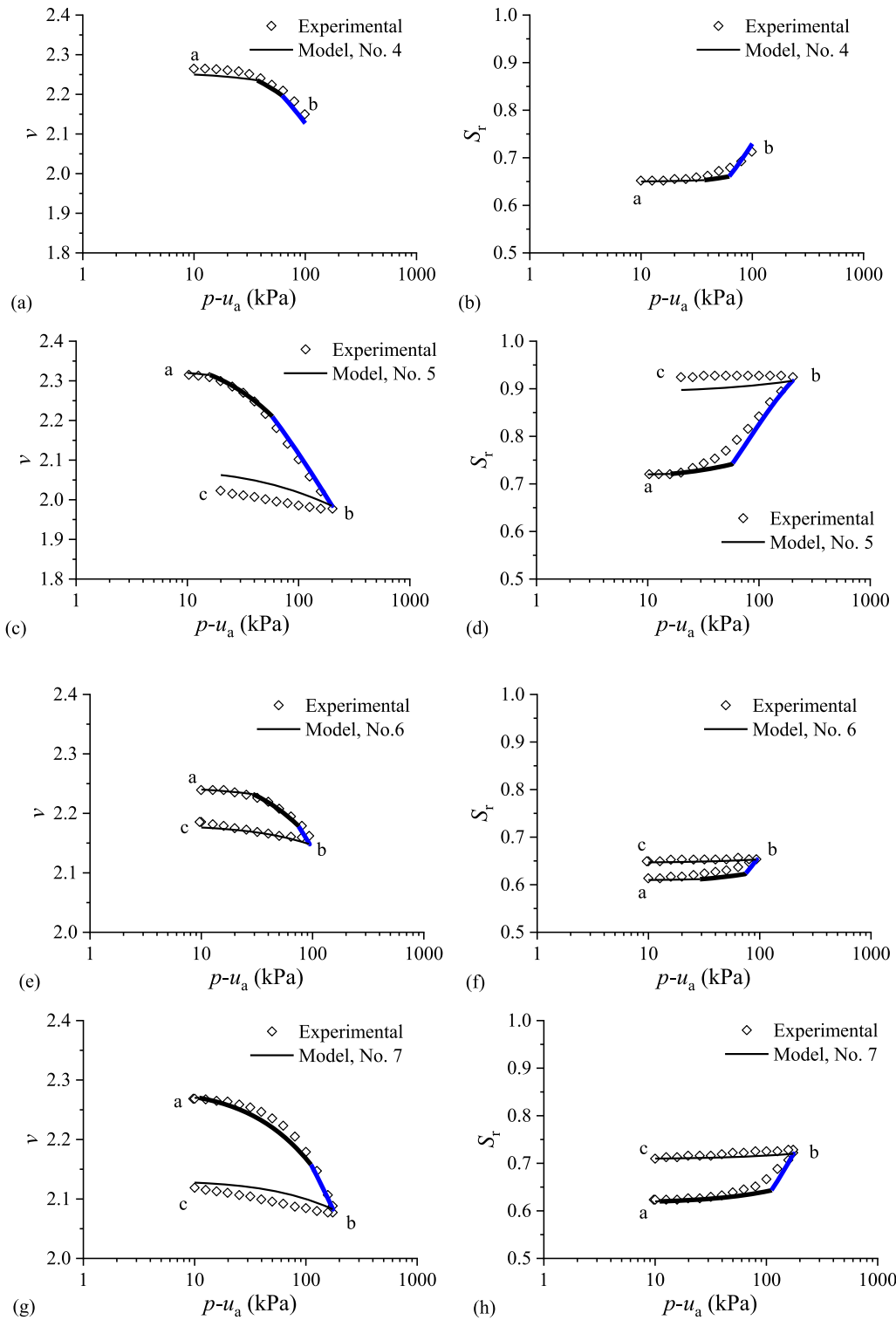
Fig. 10 Comparisons between the measured and predicted results for bentonite–kaolin mixture: **a** specific volume for No. 4; **b** degree of saturation for No. 4; **c** specific volume for No. 5; **d** degree of saturation for No. 5; **e** specific volume for No. 6; **f** degree of saturation for No. 6; **g** specific volume for No. 7; **h** degree of saturation for No. 7; Note: Model predictions are plotted in solid lines, the width of the line indicates the mechanical state of unsaturated soils, thin line for elastic state and thick line for plastic state; the color of the line indicates the hydraulic state of unsaturated soils, black for elastic state, blue for wetting state and red for drying state (not existed). This notification is also applicable to Fig. 11 and Fig. 13
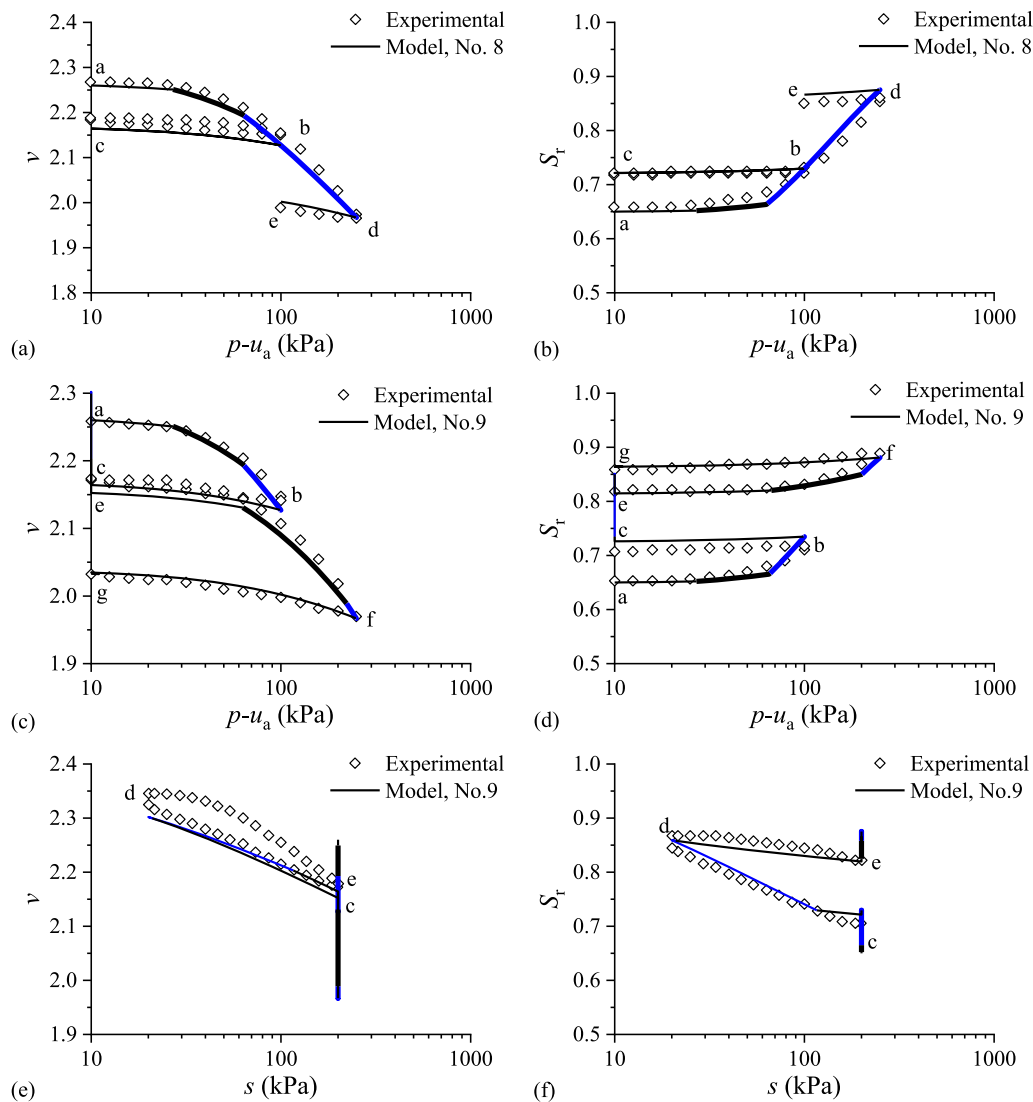
Fig. 11 Comparisons between the measured and predicted results for bentonite–kaolin mixture: **a** void ratio for No. 8; **b** degree of saturation for No. 8; **c** void ratio (with mean net stress) for No. 9; **d** degree of saturation (with mean net stress) for No. 9; (**e**) void ratio (with matric suction) for No. 9; **f** degree of saturation (with matric suction) for No. 9

6 Validation of hydraulic hypersurface

In this subsection, the influence of void ratio on SWCC is validated against experimental datasets. The soils types and model parameters for hydraulic hypersurfaces are listed in Table 2.

Comparisons between the model predictions and experimental data of the hydraulic hypersurface for soils No. 1 to No. 3 are plotted in Fig. 9. It can be seen from Fig. 9 that the hydraulic hypersurface given by Eq. 32 shows good fit with experimental data sets. In addition, Fig. 9c indicates that the model is able to describe main drying hydraulic hypersurface in a wide suction range, from 0.01 kPa to 1×10^6 kPa.

7 Validation of the hydromechanical model

Sharma [22] has conducted several isotropic loading/unloading tests on bentonite–kaolin. Those tests are carefully conducted with measurement of specific volume v, degree of saturation S_r, mean net stress $p - u_a$ and matric suction s. These tests are used to validate the proposed model. The model parameters for bentonite–kaolin are listed in Table 3.

The stress paths of the experiments (No. 4– No. 9) are listed in Table 4. The tests include loading/unloading tests under different matric suction levels. The test results and model predictions for unsaturated soils (No. 4– No. 7) are plotted in Fig. 10. Model predictions of the specific volume ($v = e + 1$) and degree of saturation with applied mean net
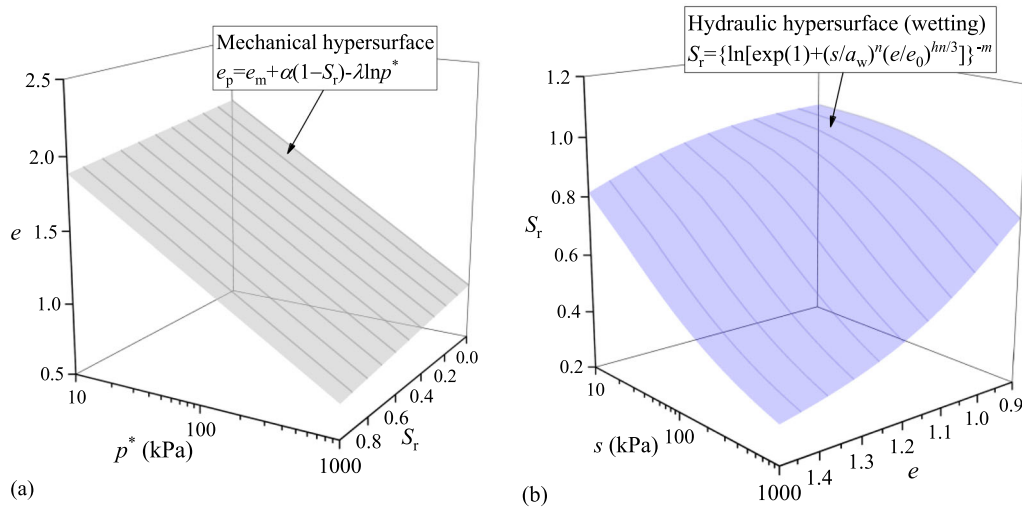
Fig. 12 The state boundary hypersurface of bentonite–kaolin during mechanical cycles [22]: **a** mechanical hypersurface; **b** Main wetting hydraulic hypersurface

Table 5 Model parameters for bentonite–kaolin under hydraulic cycling [22]

No	Hydraulic parameters						Mechanical parameters				
	a_d(kPa)	a_w(kPa)	m	n	h	κ_s	e_m	α	λ	κ	β
10	–	450	0.78	0.90	25.00	0.03	1.67	0.96	0.13	0.05	0
11	–	450	0.78	0.90	25.00	0.03	1.67	0.96	0.13	0.05	0
12	–	290	0.78	0.90	25.00	0.03	–	–	–	0.08	0.45
13	–	290	0.78	0.90	25.00	0.03	1.59	1.1	0.13	0.05	0

Note: No. 10–No. 13 indicate the original test 8, test 16, test 2 and test 1 in Sharma's [22] paper

stress in Fig. 10 show reasonable agreement with experimental data. The used model parameters are the same except little discrepancy in the value of e_m. The parameters a_d and β are not used, because neither main drying nor wetting collapse occurred during those tests.

The test results and model predictions for unsaturated soils (No. 8– No. 9) are plotted in Fig. 11. Predictions of the specific volume and degree of saturation in Fig. 11 show reasonable agreement with experimental data. The initial states for No. 8 and No. 9 are similar. The two loading–unloading stages for No. 8 and No. 9 are the same. However, there is an additional wetting–drying cycle c–d–e for No. 9, where a significant increase in the degree of saturation occurred due to hydraulic hysteresis. During the second isotropic loading stage e–f, yield occurred at a mean net stress lower than the value of 100 kPa previously applied. This phenomenon identifies the inward movement of LC yield surface with increase in degree of saturation. The inward movement of LC yield surface was not occurred for No. 8 which had not been subjected to a wetting–drying cycle.

The parameters listed in Table 2 show little discrepancy except in e_m. This indicates the correctness of the proposed model. The mechanical hypersurface ($e_m = 2.46$) and the hydraulic hypersurface are plotted in Fig. 12. The grid lines in Fig. 12a indicate the NCLs in the $e - \ln p^*$ plane. The grid lines in Fig. 12b indicate the SWCCs in the $S_r - \ln s$ plane. The two hypersurface can reflect the influence of degree of saturation on NCLs and the influence of void ratio on SWCCs.

Table 6 Stress path for bentonite–kaolin under hydraulic cycling [22]

No	$p - u_a$(kPa)	s(kPa)
10	10	$300 \rightarrow 20 \rightarrow 300$
	$10 \rightarrow 175$	300
11	10	$400 \rightarrow 20 \rightarrow 400$
12	50	$400 \rightarrow 100 \rightarrow 400$
13	10	$400 \rightarrow 50 \rightarrow 380 \rightarrow 0 \rightarrow 370$

Note: There are two loading stages for No. 10, a wetting–drying cycle followed by a mechanical loading stage
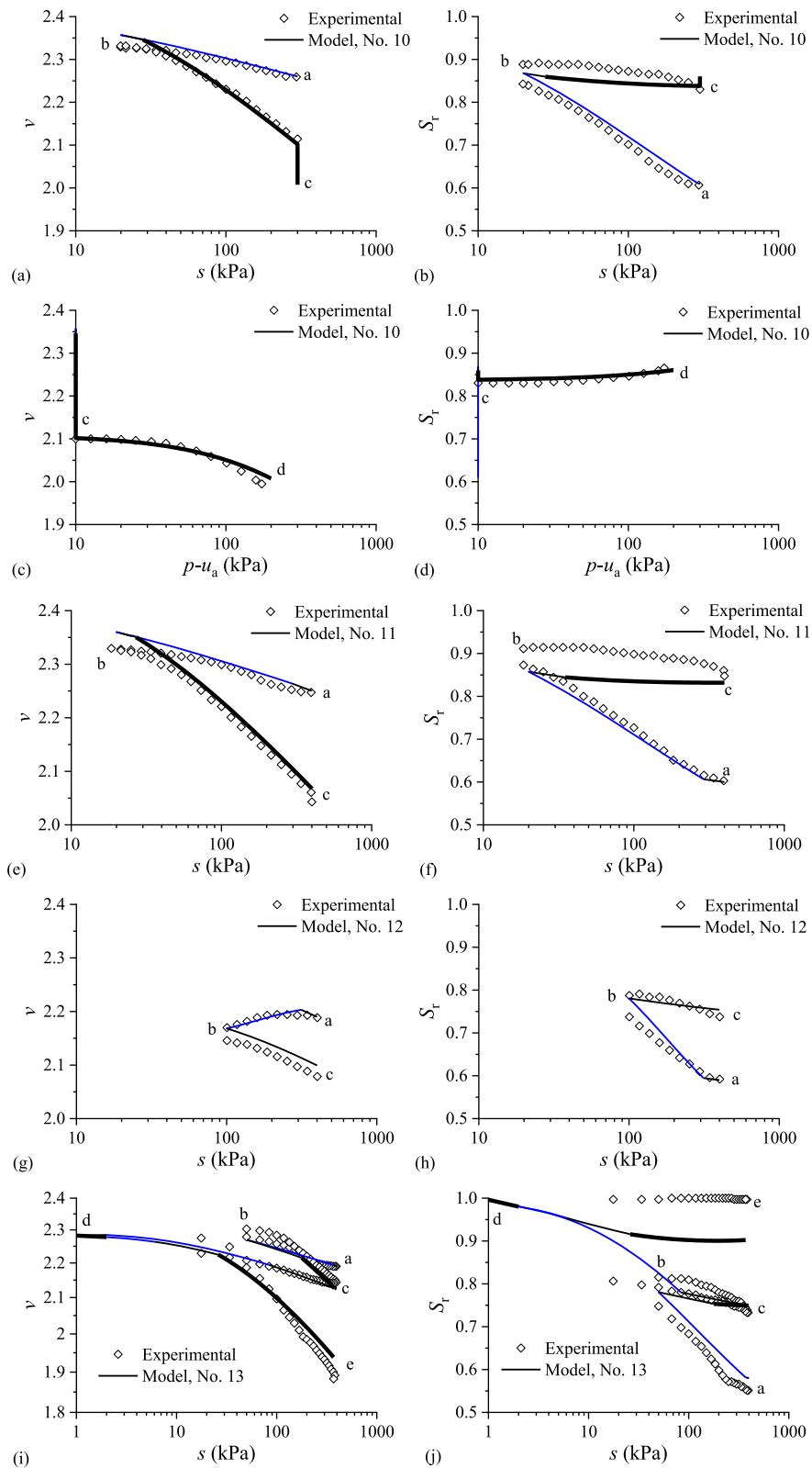
Fig. 13 Comparisons between the measured and predicted results for bentonite–kaolin mixture: **a** specific volume (with matric suction) for No. 10; **b** degree of saturation (with matric suction) for No. 10; **c** specific volume (with mean net stress) for No. 10; **d** degree of saturation (with mean net stress) for No. 10; **e** specific volume for No. 11; **f** degree of saturation for No. 11; **g** specific volume for No. 12; **h** degree of saturation for No. 12; **i** specific volume for No. 13; **j** degree of saturation for No. 13

Sharma [22] had also conducted several hydraulic cycling tests on bentonite–kaolin. These tests are also used to validate the proposed model. The model parameters for bentonite–kaolin are listed in Table 5.

The stress paths of the experiments (No. 10– No. 13) are listed in Table 6. The tests are wetting–drying tests under different mean net stress levels. The test results and model predictions for bentonite–kaolin (No. 10–No. 13) are plotted in Fig. 13.

As shown in Fig. 13, the model predictions show good agreement with experimental data. Especially, wetting collapse occurred for No. 12, where an irreversible increase of volumetric strain is accompanied by an irreversible increase of degree of saturation. This phenomenon identifies the shape of the mechanical scanning lines proposed in Sect. 2.2. However, there are two points needed to be noticed. Firstly, the model parameters listed in Table 5 show little discrepancy with the parameters listed in Table 3, the reason will be discussed in the discussion section. Secondly, the predicted degree of saturation for No.13 Fig. 10 j does not fit well with the experimental data in the d-e stage. This is caused by the using a constant slope of the hydraulic scanning line, it is better to let the value of κ_s tends to zero as S_r approaches 1. Future work may give a more detailed description of the hydraulic scanning lines.

8 Discussion

Based on state boundary hypersurfaces and scanning lines, the proposed hydromechanical model can capture some important features of unsaturated soils. The variation of degree of saturation caused by the variation of matric suction and by the variation of void ratio can be well reflected in the model. Especially, by mechanical hypersurface Eq. 33, the influence of degree of saturation on LC yield surface is expressed in a full form rather than an incremental form. This makes it much easier to judge the mechanical state of the unsaturated soil and much easier to implement the constitutive model. However, there are two questions needed to be discussed here.

One question is that the model parameters listed in Table 5 show little discrepancy with the parameters listed in Table 3. The three mechanical shape parameters α, λ, κ show different values in the mechanical cycling tests and in the hydraulic cycling tests. This may be caused by choosing the effective stress as a stress variable to build the mechanical surface and the mechanical scanning lining line.

The mechanical cycling and the hydraulic cycling show different values of shape parameters of mechanical hypersurface and mechanical scanning line. This may

indicate that the variation of void ratio caused by the variation of mean net stress is not equal to that caused by the variation of matric suction in the context of effective stress. In other words

$$(de)_{p-u_a} = \frac{\overline{\lambda}[d(p - u_a) + sdS_r]}{p^*} \neq (de)_s = \frac{\overline{\lambda}(sdS_r + S_r ds)}{p^*}$$

$$(44)$$

where $\overline{\lambda}$ is the slope of curve of $e - p^*$ in semi-log plot.

The experimental data of No. 10 on bentonite–kaolin [22] may validate this assumption. The variation of void ratio with effective stress of No. 10 is plotted in Fig. 14. As can be seen in Fig. 14, a wetting–drying cycle (blue dots) is followed by a mechanical loading stage (black dots). The slope of $e - \ln p^*$ in the wetting–drying stage is similar to the value of κ and λ listed in Table 5. The slope of $e - \ln p^*$ in the mechanical loading stage is similar to the value of λ listed in Table 3. Besides, the slope of $e - \ln p^*$ in the mechanical loading stage shows a deeper slope than that in the wetting–drying stage. This indicates that in the context of effective stress, mean net stress contributes more to soil deformation. The effective stress may be modified to give a general expression to describe deformation. Otherwise, the deformation of unsaturated soil should be control separately by two stress variables, such as mean net stress and matric suction. In this case, two more parameters may be needed to build the model, the mechanic scanning lines and the mechanic hypersurface may be given by

$$de = \frac{\kappa_a d(p - u_a)}{(p - u_a)} + \frac{\kappa_b ds}{s} + \beta dS_r \tag{45}$$

$$e_p = e_m - \alpha S_r - \lambda_a \ln(p - u_a) - \lambda_b \ln s \tag{46}$$

Of course, the reasonability of Eq. 45 and Eq. 46 needs to be validated by experimental data.

The other question is that this model is limited to isotropic loading case. Deviatoric loading tests are beyond the scope of this paper. However, if more triaxial experimental data available, this model can be extended to deviatoric
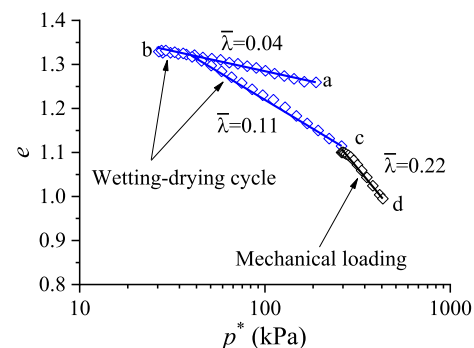

Fig. 14 The variation of void ratio with effective stress for No. 10 on bentonite–kaolin [22]

stress state. The mechanical hypersurface may be expressed as

$$e_p = e_p(p^*, q, S_r) \; or \; e_p = e_p(p - u_a, s, q, S_r) \qquad (47)$$

The shear strain may be obtained by associated or nonassociated flow rule. Of course, the premise of proposing an extended model is that there are relevant experimental data with measurements of $(p - u_a, s, q, S_r, e)$ datasets.

9 Conclusion

A general expression of the hydraulic hypersurface is proposed (Eq. (21)) based on the evolution of PSD. Two different air-entry suction is used for the main drying hydraulic hypersurface and the main wetting hydraulic hypersurface. The elastic hydraulic behavior can be expressed by scanning lines between the two hydraulic hypersurfaces. Besides, through mechanical hypersurface Eq. 33, the influence of degree of saturation on LC yield curve is expressed in total form instead of in incremental form. It becomes much easier to judge the mechanical state of unsaturated soils. The elastic mechanical behavior can be expressed by scanning lines below the mechanical hypersurface. Based on these hypersurfaces and scanning lines, an elastoplastic hydromechanical constitutive model for unsaturated soils is proposed. A large number of experimental data were used to validate the model. The model is open to improvement when more triaxial experiment data are available.

Data availability Some or all data, models or code that support the findings of this study are available from the corresponding author upon reasonable request.

Declarations The authors declare that they have no known competing financial interests or personal relationships that could have appeared to influence the work reported in this paper.

References

1. Alonso EE, Gens A, Josa A (1990) A constitutive model for partially saturated soils. Geotechnique 40(3):405–430
2. Alonso EE, Vaunat J, Gens A (1999) Modelling the mechanical behaviour of expansive clays. Eng Geol 54(1–2):173–183
3. Cheng Q et al (2019) A new water retention model that considers pore non-uniformity and evolution of pore size distribution. Bull Eng Geol Env 78(7):5055–5065
4. Chiu CF, Ng CWW (2003) A state-dependent elasto-plastic model for saturated and unsaturated soils. Geotechnique 53(9):809–829
5. Chiu CF, Ng CWW (2012) Coupled water retention and shrinkage properties of a compacted silt under isotropic and deviatoric stress paths. Can Geotech J 49(8):928–938
6. Fredlund DG, Xing AQ (1994) Equations for the soil-water characteristic curve. Can Geotech J 31(4):521–532
7. Gallipoli D, Wheeler SJ, Karstunen M (2003) Modelling the variation of degree of saturation in a deformable unsaturated soil. Geotechnique 53(1):105–112
8. Ghasemzadeh H, Amiri SAG (2013) A hydro-mechanical elastoplastic model for unsaturated soils under isotropic loading conditions. Comput Geotech 5191–100
9. Hu R et al (2013) A water retention curve and unsaturated hydraulic conductivity model for deformable soils: consideration of the change in pore-size distribution. Geotechnique 63(16):1389–1405
10. Hu R et al (2014) A constitutive model for unsaturated soils with consideration of inter-particle bonding. Computers and Geotechnics 59127–59144
11. Huang SY, Barbour SL, Fredlund DG (1998) Development and verification of a coefficient of permeability function for a deformable unsaturated soil. Can Geotech J 35(3):411–425
12. Khalili N, Habte MA, Zargarbashi S (2008) A fully coupled flow deformation model for cyclic analysis of unsaturated soils including hydraulic and mechanical hystereses. Comput Geotech 35(6):872–889
13. Liu WH, Yang Q, Sun XL (2020) Hydro-mechanical constitutive model for overconsolidated unsaturated soils. Eur J Environ Civ Eng 24(11):1802–1820
14. Lloret-Cabot M, Sanchez M, Wheeler SJ (2013) Formulation of a three-dimensional constitutive model for unsaturated soils incorporating mechanical-water retention couplings. Int J Numer Anal Meth Geomech 37(17):3008–3035
15. Lloret-Cabot M, Wheeler SJ, Sanchez M (2017) A unified mechanical and retention model for saturated and unsaturated soil behaviour. Acta Geotech 12(1):1–21
16. Muraleetharan KK et al (2009) An elastoplatic framework for coupling hydraulic and mechanical behavior of unsaturated soils. Int J Plast 25(3):473–490
17. Ng CWW, Peprah-Manu D, Zhou C (2023) Effects of pore structure on the hysteretic water retention behaviour of silty sand at different stresses. Acta Geotech 18(12):6489–6504
18. Ng CWW, Zhou C (2014) Cyclic behaviour of an unsaturated silt at various suctions and temperatures. Geotechnique 64(9):709–720
19. Nuth M, Laloui L (2008) Advances in modelling hysteretic water retention curve in deformable soils. Comput Geotech 35(6):835–844
20. Romero E, Gens A, Lloret A (1999) Water permeability, water retention and microstructure of unsaturated compacted Boom clay. Eng Geol 54(1–2):117–127
21. Salager S et al (2013) Investigation into water retention behaviour of deformable soils. Can Geotech J 50(2):200–208
22. Sharma R (1998) Mechanical behavior of unsaturated highly expansive clays. PhD dissertation, University of Oxford, UK
23. Sheng D, Fredlund DG, Gens A (2008) A new modelling approach for unsaturated soils using independent stress variables. Can Geotech J 45(4):511–534
24. Sheng D, Sloan SW, Gens A (2004) A constitutive model for unsaturated soils: thermomechanical and computational aspects. Comput Mech 33(6):453–465
25. Sheng DC, Zhou AN (2011) Coupling hydraulic with mechanical models for unsaturated soils. Can Geotech J 48(5):826–840

26. Song, Z.Y., Z.H. Zhang, and X.L. Du (2024) A generalized water retention model in a wide suction range considering the initial void ratio and its verification. Computers and Geotechnics 166.

27. Sun DA et al (2007) A three-dimensional elastoplastic model for unsaturated compacted soils with hydraulic hysteresis. Soils Found 47(2):253–264

28. Sun DA, Sheng DC, Sloan SW (2007) Elastoplastic modelling of hydraulic and stress-strain behaviour of unsaturated soils. Mech Mater 39(3):212–221

29. Sun DA, Sheng DC, Xu YF (2007) Collapse behaviour of unsaturated compacted soil with different initial densities. Can Geotech J 44(6):673–686

30. Sun WJ, Sun DA (2012) Coupled modelling of hydro-mechanical behaviour of unsaturated compacted expansive soils. Int J Numer Anal Meth Geomech 36(8):1002–1022

31. Tanaka H et al (2003) Pore size distribution of clayey soils measured by mercury intrusion porosimetry and its relation to hydraulic conductivity. Soils Found 43(6):63–73

32. Tarantino A, De Col E (2008) Compaction behaviour of clay. Geotechnique 58(3):199–213

33. Tsiampousi A, Zdravkovic L, Potts DM (2013) A three-dimensional hysteretic soil-water retention curve. Geotechnique 63(2):155–164

34. Wang Q et al (2013) Investigation of the hydro-mechanical behaviour of compacted bentonite/sand mixture based on the BExM model. Comput Geotech 5446–5452

35. Wang Y et al (2022) A critical saturated state-based constitutive model for volumetric behavior of compacted bentonite. Can Geotech J

36. Wei XS et al (2024) Exploring the effect of volume change on capillary soil water retention in an undisturbed silty clay: an experimental and modeling approach. Acta Geotechnica

37. Wheeler SJ, Sharma RS, Buisson MSR (2003) Coupling of hydraulic hysteresis and stress-strain behaviour in unsaturated soils. Geotechnique 53(1):41–54

38. Wheeler SJ, Sivakumar V (1995) An elasto-plastic critical state framework for unsaturated soil. Geotechnique 45(1):35–53

39. Wheeler SJ, Sivakumar V (2000) Influence of compaction procedure on the mechanical behaviour of an unsaturated compacted clay. Part 2. shearing and constitutive modelling. Geotechnique 50(4):369–376

40. Yao YP et al (2023) Unified hardening (UH) model for unsaturated expansive clays. Acta Geotechnica

41. Zhou C, Ng CWW (2015) A thermomechanical model for saturated soil at small and large strains. Can Geotech J 52(8):1101–1110

42. Zhou C, Ng CWW (2018) A new thermo-mechanical model for structured soil. Geotechnique 68(12):1109–1115

43. Zhou C, Tai P, Yin JH (2020) A bounding surface model for saturated and unsaturated soil-structure interfaces. Int J Numer Anal Meth Geomech 44(18):2412–2429

44. Zhou AN et al (2012) Interpretation of unsaturated soil behaviour in the stress-saturation space II: Constitutive relationships and validations. Comput Geotech 43111–123

45. Zhou AN et al (2018) Including degree of capillary saturation into constitutive modelling of unsaturated soils. Comput Geotech 9582–98

46. Zhou C, Ng CWW (2016) Effects of Temperature and Suction on Plastic Deformation of Unsaturated Silt under Cyclic Loads. J Mater Civil Eng 28(12)

47. Zhou AN et al (2012) Interpretation of unsaturated soil behaviour in the stress - Saturation space, I: Volume change and water retention behaviour. Comput Geotech 43178–187

48. Zhou C, Ng CWW (2014) A new and simple stress-dependent water retention model for unsaturated soil. Comput Geotech 62216–222